

AC to DC bridgeless SEPIC converter-based fuel cell emulator

Ashish Prajapati¹, Tripurari Das Gupta², Kalpana Chaudhary¹

¹Department of Electrical Engineering, Indian Institute of Technology (BHU), Varanasi, India

²Departemnt of Electrical Engineering, Nalanda College of Engineering, Nalanda, India

Article Info

Article history:

Received Jan 16, 2024

Revised Mar 28, 2024

Accepted Apr 18, 2024

Keywords:

Clean energy

DSP control

Fuel cell

Fuel cell emulator

Sepic converter

ABSTRACT

Fuel cell (FC) technology is still in a growing phase and intensive research is required for its wider applications. However, the high cost of the FC stack is a major hurdle for researchers. This paper presents a new method of FC emulation done by using a Bridgeless SEPIC converter (BSC). The key features of the designed emulator are single stage AC-DC conversion, improved efficiency and nearly unity power factor at the input side. AC-DC BSC is controlled by using the coded model to emulate the behavior of FC. The emulated FC exhibits all three characteristics activation losses, ohmic losses, and concentration losses during operation. The MATLAB/Simulink background is used to implement the FC model and compile it into a C program. The real-time mathematical model is implemented by using a DSP(TMS320F28335) controller. Analysis, modeling, and control strategy of emulated FC are presented, static and dynamic behavior is validated through the 950W laboratory developed prototype.

This is an open access article under the [CC BY-SA](https://creativecommons.org/licenses/by-sa/4.0/) license.



Corresponding Author:

Ashish Prajapati

Department of Electrical Engineering, Indian Institute of Technology (BHU)

Varanasi, India

Email: ashishprajapati.rs.eee19@iitbhu.ac.in

1. INTRODUCTION

In recent decades, there has been a growing interest in fuel cell systems (FCS) for both stationary and mobile power generation. Proton exchange membrane FCS (PEM-FCS) stand out as highly attractive options for both distributed generation (DG) and vehicle applications, thanks to their remarkable characteristics such as superior power density, utilization of solid electrolytes, minimal susceptibility to corrosion, and ability to operate efficiently at lower temperature ranges. However, several concerns remain, including the cost, size, weight, and complexity of peripheral devices [1]–[3]. FCS are intricate systems where various physical phenomena such as thermal, electrochemical, and electrical processes occur. Auxiliary components such as the hydrogen supply system for the anode, the air management system for the cathode, cooling systems, and humidifiers are essential for the proper functioning of the fuel cell stack. Optimizing these components is crucial not only for improving the performance of the FC stack itself but also for enhancing the interactions among the different auxiliaries, which are inherently nonlinear, block diagram and their equivalent circuit and converter circuit diagram as shown in Figures 1(a)-1(c).

However, the cost of the fuel cell (FC) stacks, associated with the expense of hydrogen fuel and the limited lifespan determined by no of hours used and on/off cycles, restricts their widespread use in experimentation. This limitation poses challenges, particularly when designing and validating power conditioner systems (PCS) from the output of the FC. These PCS typically include components such as DC/DC step-up converters, bidirectional dc/dc converters (if a buffer energy source is present), and DC/AC inverters. Currently, most PCSs are primarily tested using a constant DC source with a first-order delay. Various high-gain converter topologies are discussed for renewable applications [3], [4]. Additionally, the size of auxiliary

equipment can often exceed the dimensions of the FC, resulting in increased associated costs and space requirements. Hence, it becomes imperative to devise a solution for conducting experimentation without using a physical fuel cell system (FCS), especially in the first stages [5], [6]. Considering all circuit parameters for substituting the FC stack with a hardware system capable of accurately mimicking its behavior. By utilizing an emulator, the real FC stack can be temporarily replaced, allowing for the study and setup of the remaining components of the FCS, such as auxiliaries, interfaces, and charges [7].

Various FC emulators have been reported using buck converter [8], [9], boost converter [10], interleaved synchronous buck converter [11], microcontroller-based emulator [12], multiphase interleaved dc-dc [13]. All these emulators are developed using a dc-dc converter. As dc supply requires battery banks or ac-dc converter which increases the size and cost of FC emulators. In the laboratory, as AC supply is readily available, a single-phase bridgeless ac-dc converter can be employed. In this work, a Bridgeless SEPIC converter (BSC) based on FC is developed. Instead of a complex equivalent circuit model (ECM), a more versatile ac-dc converter-based FC emulator can be used. As it can incorporate the physical and chemical behavior of PEMFC by implementing its mathematical model accurately. The increasing FC implementation in different systems has made the design, testing, and fault diagnosis of these systems essential with FC as the source. The equivalent circuit model (ECM) is suggested by many researchers to analyze the behavior of FCs given in [14]–[17]. In addition to high complexity, the ECM cannot exhibit an accurate transient behavior nor changes in parameters in running conditions [18], [19]. The model gives a result for steady state, dynamic modeling, control of FC and nonlinear equation presented in reference [20]. DSP-based FC simulation applies a linear relationship between the output voltage and current of the FC. Ignoring the non-linearity of FC improves the both steady state and transient response of the FC. A parallel RC circuit in equivalent impedance replaces the activation and concentration drop of the cell.

This paper presents the AC-DC BSC FC emulator, which has approximately a unity power factor of 0.994 on the input side. The implemented model exactly follows the real FC Nernst equations for reversible voltage (open circuit voltage) and irreversible voltage drop (activation, concentration, and ohmic drop). FC emulator follows dynamic characteristics of real PEMFC. The emulated output voltage of the FC emulator is adjustable, controllable, and scalable. This makes it suitable for testing and laboratory use. This paper is organized as follows, section 2 describes the modeling of the fuel cell, section 3 depicts the BSC converter design and stability analysis, section 4 shows the fuel cell emulation, DSP, and control strategy, analyzes and discuss the result and finally conclude the paper in section 5.

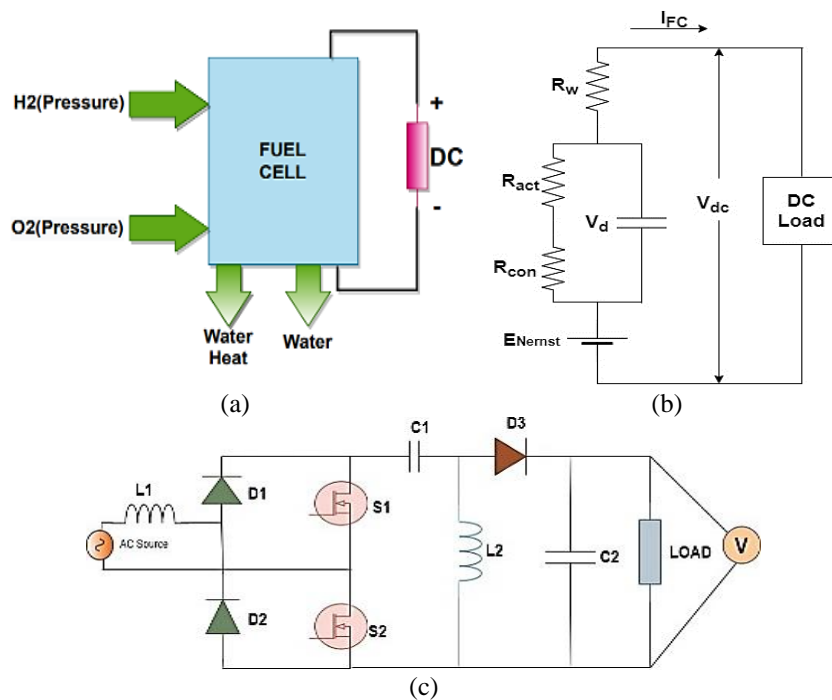


Figure 1. Block diagram and circuit diagram: (a) fuel cell, (b) circuit diagram of fuel cell, and (c) circuit diagram of BSC

2. FUEL CELL MODELLING

FC transforms chemical energy into electrical energy through the redox reaction. Hydrogen oxidized on anode electrochemically produces proton H^+ and electron e^- . Proton move through membrane to cathode and electron are compulsively move to outer closed-loop circuit, generating electric current I_o . On cathode terminal, electrons flow through outer circuit and protons move through the membrane combined with O_2 molecule to produce heat and water. FC modeling and equations are referred to as [21], [22]. Oxidation and reduction reactions are given by (1) and (2).



2.1. Terminal voltage of fuel cell

The terminal voltage of a fuel cell is the voltage available from the cell's electrodes when it's connected to an external circuit and a load. It's a measure of the cell's electrochemical potential, determined by the chemical reactions occurring within the cell. The terminal voltage depends on various factors such as the type of fuel cell, operating conditions (temperature and pressure), and the load connected to it. The terminal voltage of FC is obtained after various drops of FC like concentration drop, ohmic drop, and activation drop are given in (3) and (4).

$$V_{FC} = V_{Nearst} - V_{act} - V_{FC} - V_{ohmic} - V_{con} \quad (3)$$

$$V_s = nV_{FC} \quad (4)$$

2.2. Nernst voltage

Nernst voltage of the FC depends on the pressure of individual species, which is calculated by using mass action flow conservation. The electrochemical equation is represented by the parallel RC circuit in Figure 1(b). The voltage that appears across the capacitor of the parallel RC circuit is equivalent to the partial pressure P_i of the gases as given in (5),

$$E_{Nearst} = -\frac{\Delta H^0}{2F} + \frac{\Delta S^0}{2F} (T_{fc} - T_{fco}) + \frac{RT_{fc}}{2F} [\ln(P_{H_2} + .5 * (P_{O_2}))] \quad (5)$$

where E_{Nearst} is thermodynamic potential of each cell, $R=8.314$ KJ/Kmol, $T=25^\circ\text{C}$ is temperature of FC during operation, $F=96486$ C/mol is faradays constant, P_{H_2} , P_{O_2} is hydrogen and oxygen partial pressure. Putting all values to get a final (6) for the Nernst voltage

$$E_{Nearst} = 1.229 - 0.85 * 10^{-3} (T_{fc} - 298.15) + 4.31 * 10^{-5} * T [\ln(P_{H_2} + .5 * (P_{O_2}))] \quad (6)$$

2.3. Activation voltage drop

Activation losses are related to electrochemical reaction kinetics in FC. These losses occur due to charge transfer causing the slowness of the reaction taking place on the surface of the electrode. Certain temperatures due to low current density and catalyst effectiveness cause polarization losses. Activation potential is given by the Butler Volmer equation. This potential change with temperature and current density can be expressed as (7).

$$V_{act} = -[\zeta_1 + \zeta_2 * T * \zeta_3 * \ln(C_{O_2}) + \zeta_4 * T * \ln(I_{fc})] \quad (7)$$

2.4. Ohmic losses

This drop is the same as resistance drop, which occurs due to charge flow from one electrode to other electrodes, resistance suffered by the charge moving between these electrodes causes ohmic losses. Electrolytes work as the resistance between the electrodes. Reduction in voltage at the terminal of the FC is due to ohmic losses and this ohmic loss is expressed as electronic resistance (R_{elect}) and ionic resistance (R_{ionic}) of the FC. This can be written as (8).

$$V_{ohmic} = I_{fc} * (R_{ionic} + R_{elect}) \quad (8)$$

R_{ionic} is electrolyte resistance of solution in FC, and R_{elect} denote electrical resistance of bipolar plates.

2.5. Concentration losses

Concentration loss occurs due to a change in concentration of a reactant at the surface of the electrodes during the operation of FC. This concentration loss affects the voltage of FC presented in (9).

$$V_{con} = -\frac{RT}{nF} * \ln\left(1 - \frac{I_f c}{I_L}\right) \quad (9)$$

Where I_L denote the current density of the cell.

3. BRIDGELESS SEPIC CONVERTER

Lower input current ripple and in comparison, to other AC/DC converters has a less no. of switches. That is why mitigates the losses of the converter and the performance of the converter improved Figure 1(c). Designing parameter of this converter is referred to as [23]–[25].

3.1. Converter design and stability analysis

3.1.1. Converter design

For designing circuit parameters, it is easier to work with per-phase quantities for the calculations. Using these parameters, you can figure out the average voltage. Per phase voltage (V_{rms}) ≈ 220 V, maximum phase voltage (V_m) ≈ 310 V, average voltage ($V_{in(avg)}$) $= \frac{2\sqrt{2}V_m}{\pi} = 198$ V, also Duty Cycle (D) $= \frac{V_o}{V_o + V_{in(avg)}} = 0.476$, $V_{in(avg)} = \frac{P_o}{V_{in(avg)}} = 4.79$ A. Therefore, input inductor $L_1 = \frac{V_m D T_s}{\Delta I_{L1}} = 3.84$ mH, where V_m is the peak of supply voltage (i.e. $220\sqrt{2}$ V), T_s is the switching period $\frac{1}{f_s}$, where f_s is the switching frequency = 40 kHz.

$$\begin{aligned} (K_a)_{critical} &= \frac{1}{2(1+M)^2} \\ &= \frac{1}{2[(V_o/V_m)+1]^2} = 0.201 \end{aligned}$$

As $K_a < (K_a)_{critical}$. As a result, K_a is taken as 0.15. After calculation of K_a , the equivalent inductance of the circuit can be determined by using the equation given below:

$$L_{eq} = \frac{R_o T_s K_a}{2} = \frac{35 * 2.5 * 10^{-5} * 0.15}{2} = 65.625 \mu\text{H}$$

Hence, the value of output inductor can be calculated as $L_o = \frac{L_i * L_{eq}}{L_{eq} - L_i} = 666.6 \mu\text{H}$. In this work, an inductor value of $200 \mu\text{H}$ is chosen because the output inductor is designed to be in DICM. The filter equation is used to get the capacitor's value. Calculating capacitance C_1 requires taking the frequency at the logarithmic mean of 10^5 Hz and 50 Hz ($f_s = 1414.164$ Hz) [23].

$$C_1 = \frac{1}{(2 * \pi * 1414.164)^2 (3000 + 200) 10^{-6}} = 4.08 \mu\text{F}$$

Capacitors are chosen at the commercially available value of $10 \mu\text{F}$ while taking the amount of leakage current into consideration. The circuit's designed parameters are listed in Table 1.

The value of the output capacitor is taken as $1000 \mu\text{F}$ as it is high enough to bring down the voltage ripples to approximately 1% of the output voltage at the rated load.

Table 1. Designed converter parameter

Parameters	Value	Parameters	Value
Input Inductor L_1	3.84 mH	Capacitor C_2	1000 μF
Inductor L_2	200 μH	Resistor R_L	35 Ohm
Capacitor C_1	10 μF	Frequency f_s	40 Hz

3.1.2. Stability analysis

The stability of a system refers to its capability to yield bounded output in response to a bounded input. The general state space representation of a system can be expressed as $\dot{x}(t) = Ax(t) + Bu(t)$ and $y(t) = Cx(t) + Du(t)$. The state-space equations describe the behavior of the step-up converter during both its ON and OFF states.

$$\dot{x}(t) = A_1x(t) + B_1x(t)$$

$$\begin{pmatrix} \dot{i}_{L1} \\ \dot{i}_{L2} \\ \dot{v}_{c1} \\ \dot{v}_{c2} \end{pmatrix} = \begin{pmatrix} 0 & 0 & 0 & 0 \\ 0 & 0 & \frac{1}{L_2} & 0 \\ 0 & -\frac{1}{C_1} & 0 & 0 \\ 0 & 0 & 0 & \frac{-1}{R_oC_2} \end{pmatrix} \begin{pmatrix} i_{L1} \\ i_{L2} \\ v_{c1} \\ v_{c2} \end{pmatrix} + \begin{pmatrix} \frac{1}{L_1} \\ 0 \\ 0 \\ 0 \end{pmatrix} (v_g)$$

$$\dot{x}(t) = A_2x(t) + B_2x(t)$$

$$\begin{pmatrix} \dot{i}_{L1} \\ \dot{i}_{L2} \\ \dot{v}_{c1} \\ \dot{v}_{c2} \end{pmatrix} = \begin{pmatrix} 0 & 0 & \frac{-1}{L_1} & \frac{-1}{L_1} \\ 0 & 0 & 0 & \frac{-1}{L_2} \\ \frac{1}{C_1} & 0 & 0 & 0 \\ \frac{1}{C_2} & \frac{-1}{C_2} & 0 & \frac{-1}{R_oC_2} \end{pmatrix} \begin{pmatrix} i_{L1} \\ i_{L2} \\ v_{c1} \\ v_{c2} \end{pmatrix} + \begin{pmatrix} \frac{1}{L_1} \\ 0 \\ 0 \\ 0 \end{pmatrix} (v_g)$$

$$\begin{aligned} y(t) &= C_1x(t) + D_1u(t) \\ y(t) &= C_2x(t) + D_2u(t), \end{aligned} (v_o) = \begin{pmatrix} 0 & 0 & 0 & 1 \end{pmatrix} \begin{pmatrix} i_{L1} \\ i_{L2} \\ v_c \\ v_{co} \end{pmatrix} + \begin{pmatrix} 0 \end{pmatrix} (v_g)$$

Now applying state-space averaging technique

$$\begin{aligned} A &= A_1D + A_2(1 - D) \\ B &= B_1D + B_2(1 - D) \\ A &= \begin{pmatrix} 0 & 0 & \frac{-(1-D)}{L_1} & \frac{-(1-D)}{L_1} \\ 0 & 0 & \frac{D}{L_2} & \frac{-(1-D)}{L_2} \\ \frac{(1-D)}{C_1} & \frac{-D}{C_1} & 0 & 0 \\ \frac{(1-D)}{C_2} & \frac{(1-D)}{C_2} & 0 & \frac{-1}{R_oC_2} \end{pmatrix}, B = \begin{pmatrix} \frac{1}{L_1} \\ 0 \\ 0 \\ 0 \end{pmatrix}, C = \begin{pmatrix} 0 & 0 & 0 & 1 \end{pmatrix} \\ D &= \begin{pmatrix} 0 \end{pmatrix} \end{aligned}$$

By using small-signal modeling and applying a perturbation to obtain the overall state space equation and transfer function of the converter

$$\begin{pmatrix} \widetilde{i}_{L1} \\ \widetilde{i}_{L2} \\ \widetilde{v}_{c1} \\ \widetilde{v}_{c2} \end{pmatrix} = \begin{pmatrix} 0 & 0 & \frac{-(1-D)}{L_1} & \frac{-(1-D)}{L_1} \\ 0 & 0 & \frac{D}{L_2} & \frac{-(1-D)}{L_2} \\ \frac{(1-D)}{C_1} & \frac{-(1-D)}{C_1} & 0 & 0 \\ \frac{(1-D)}{C_2} & \frac{1-D}{C_2} & 0 & \frac{-1}{R_oC_2} \end{pmatrix} \begin{pmatrix} \widetilde{i}_{L1} \\ \widetilde{i}_{L2} \\ \widetilde{v}_{c1} \\ \widetilde{v}_{c2} \end{pmatrix} + \begin{pmatrix} \frac{v_{c1} + v_{c2}}{L_1} \\ \frac{v_{c1} + v_{c2}}{L_2} \\ \frac{-(i_{L1} + i_{L2})}{C_1} \\ \frac{-(i_{L1} - i_{L2})}{C_2} \end{pmatrix} (\tilde{d})$$

The duty to output voltage transfer function $G(s)$ written in (10) is calculated by substituting all passive element values from Table 1 and duty cycle $D = 0.479$.

$$\begin{aligned} G(s) &= OLTF = \frac{\widetilde{v}_o(s)}{\widetilde{d}(s)} \\ &= \frac{-1.97 \times 10^{27} S^3 + 1.709 \times 10^{32} S^2 - 2.803 \times 10^{35} s + 1.73 \times 10^{39}}{3.76 \times 10^{22} S^4 + 1.603 \times 10^{24} S^3 + 3.714 \times 10^{30} S^2 + 1.54 \times 10^{32} S + 9.4 \times 10^{35}} \end{aligned} \tag{10}$$

It can be seen from above the transfer function that all poles, two zeros lie on the left half S-plane and one zero is located on the right half of the S-plane of the root locus. A PI controller's transfer function is,

$$G_{PI} = \frac{K_p s + K_i}{s}$$

'Ziegler–Nichols' method is used to tune the PI controller, the value of $K_p = 3.5 \times 10^{-6}$ and $K_i = 0.00579$ substitutes all values in (11) and obtain the closed-loop transfer function (CLTF) as (11).

$$CLTF = \frac{\overline{v_o(s)}}{\overline{d(s)}} = \frac{-6.904 \times 10^{21} S^4 + 5.86 \times 10^{26} S^3 + 8.14 \times 10^{27} S^2 + 4.43 \times 10^{33} s + 1.002 \times 10^{37}}{S(3.76 \times 10^{22} S^4 + 1.603 \times 10^{24} S^3 + 3.714 \times 10^{30} S^2 + 1.54 \times 10^{32} s + 9.4 \times 10^{35})} \quad (11)$$

Figure 2(a) shows the magnitude and phase plot of CLTF. The magnitude graph contains two up-down glitches caused by two pairs of complex conjugate poles. The bode diagram shows the phase margin (PM = 34.90) and gain margin (GM=12 dB), demonstrating that the system is stable. Table 2 presents a comparative analysis between the suggested fuel cell emulator and existing converter-based emulators. The converters described in references [9]-[11] utilize a buck converter, boost converter, and interleaved synchronous buck converter as the basis for the fuel cell emulator. These converters necessitate a DC power supply and exhibit moderate to high current ripple at the input side, as in references [9] and [10]. Another converter discussed in reference [13] proposes a multiphase interleaved-based fuel cell emulator, but it requires complex control mechanisms. In contrast, the proposed converter employs a single-stage AC to DC converter with simpler control and lower current ripple at the input side.

Table 2. Converter used for FC emulation list

Converter used	Supply type	Control complexity	Ripple current	Efficiency
Buck converter-based FC emulator [9]	DC	Easy	Moderate	High
Boost converter-based FC emulator [10]	DC	Easy	High	High
Interleaved synchronous buck converter [11]	DC	Easy	Less	High
Multiphase interleaved DC-DC converter-based FC emulation [13]	AC	Complex (Two-stage)	Very less	Low
Bridgeless SEPIC converter-based emulator	AC	Easy (One stage)	Very less	Moderate

4. RESULT AND DISCUSSION

4.1. Validation of the proposed emulator

The output current of BSC given to the FC MATLAB model, according to temperature, hydrogen and oxygen pressure generates a voltage which is compared to the output voltage of the converter and generates an error signal which is given to the PI controller, the output of controller given to PWM generator which generates a duty cycle.

- Operational state of the coded model of fuel cell (PEMFC) with BSC converter

i) V-I curve

In the V-I curve, voltage depends upon current, when the current is increasing then voltage decreases at a certain value of current, and voltage decreases drastically as shown in Figure 2(b). The result obtained from MATLAB is approximately the same as the real FC model.

ii) P-I curve

In the P-I curve, power increases when the current is increasing at a certain point power decreases when the current increases. The static operating point is established not only by the FC parameters but also by the load resistance, denoted as R. The performance of the PEMFC is directly affected by variations in the load resistor. Consequently, crucial characteristic curves, as depicted in Figures 2(c), are derived by assessing the model from (3), with all parameters specified in Table 1 held constant, except for the temperature.

The temperature operates within the range of $T_i = 25 \text{ }^\circ\text{C}$ to $T_f = 80 \text{ }^\circ\text{C}$, with regular step changes. Concurrently, the load resistor undergoes variations within the range of $10 < R < 90 \text{ ohm}$, where values less than 1 ohm might lead to saturation of the actual PEMFC, potentially causing damage. Figure 2(b) was generated by linearly adjusting the load resistor, with measurements and recordings taken for output voltage and current at different operating temperatures Figure 3(a). Similarly, the V-I and P-V curve is depicted in Figures 3(b) and 3(c), where the three distinct operating regions are easily identifiable in both cases.

Neglecting the impact of parasitic elements, the maximum power point is attained when the load resistor matches the equivalent resistance. In the specific scenario of $T_o = 25\text{ }^\circ\text{C}$, representing the point where harvesting the power from the PEMFC is maximized. The proposed emulator tested by varying the load. The load resistor undergoes variation within the range of 10 to 90 ohms, ensuring coverage of a significant portion of the curve points. Additionally, to enhance the emulator's flexibility, a 950 W PEMFC has been programmed into the MCU. The experimental outcomes are depicted in Figure 3(c), where it is evident that the samples obtained using the prototype closely follow the theoretical FC curve. The various phases of the emulator, as depicted in Figure 4(a), interface with the proposed converter. The algorithms illustrated in Figure 4(b) are programmed into MCU, which dynamically calculates energy losses using (3). The 8-bit word V_{AI} is fed into the DAC, generating a continuous analog signal represented as the output voltage V_O . The voltage V_{AO} is determined by the measured current. Subsequently, the constant voltage source (CVS) is regulated by signal V_c to ensure appropriate power levels, and this output voltage is then directed to the BSC based sepic converter and laboratory setup as depicted in Figure 4(c). As a standard feature, the power converter yields an output voltage equal to or greater than the input voltage. The Power Electronics Controller (PEC) supplies the load resistor with the voltage V_{PEC} . The measured current (I_m) and voltage (V_m) serve as feedback to the microcontroller unit (MCU) through ADC_1 and ADC_2 , thereby closing the loop of the system.

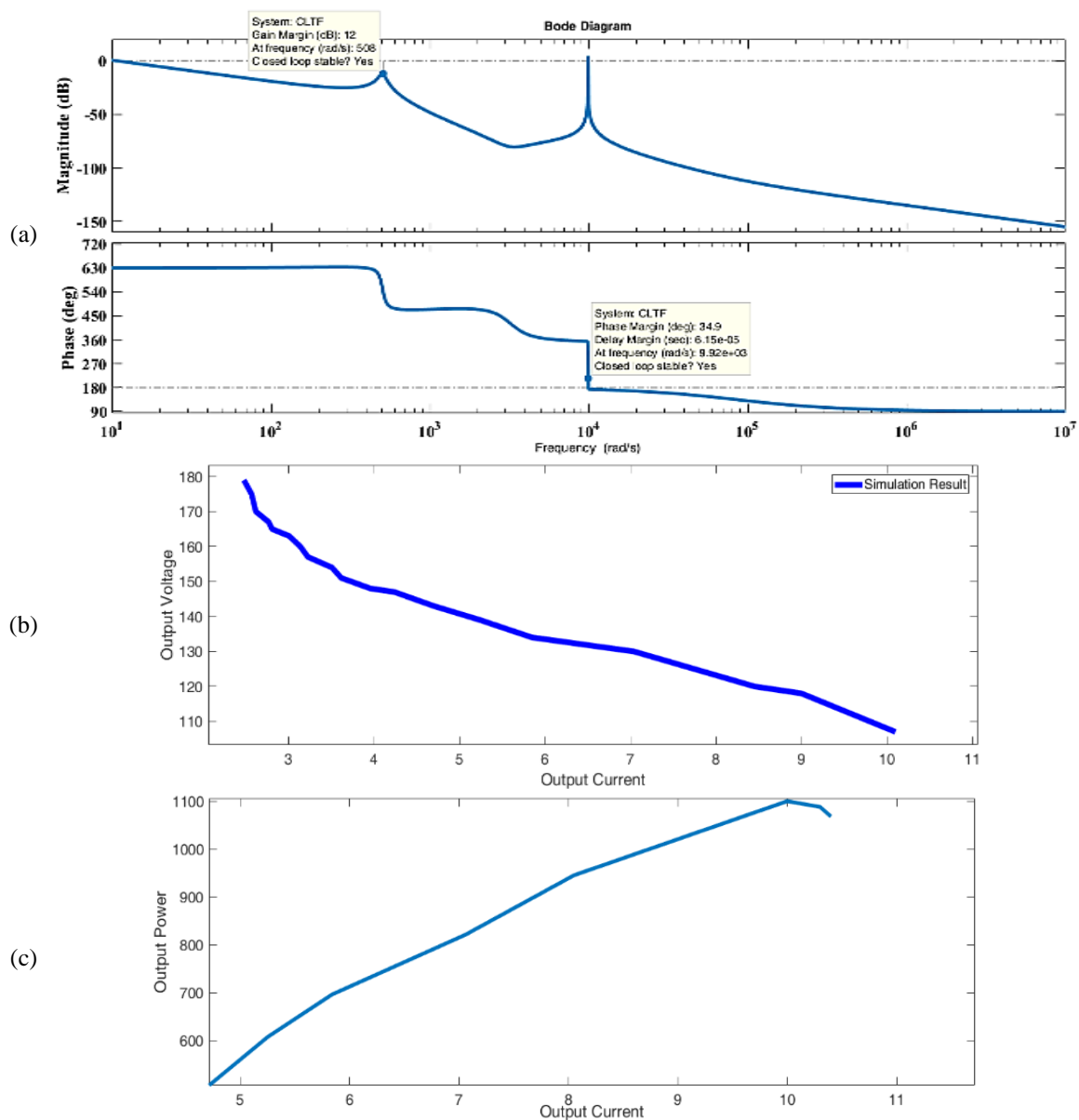


Figure 2. Characteristic of fuel cell: (a) bode plot for CLTF, (b) curve between voltage and current, and (c) curve between power and current

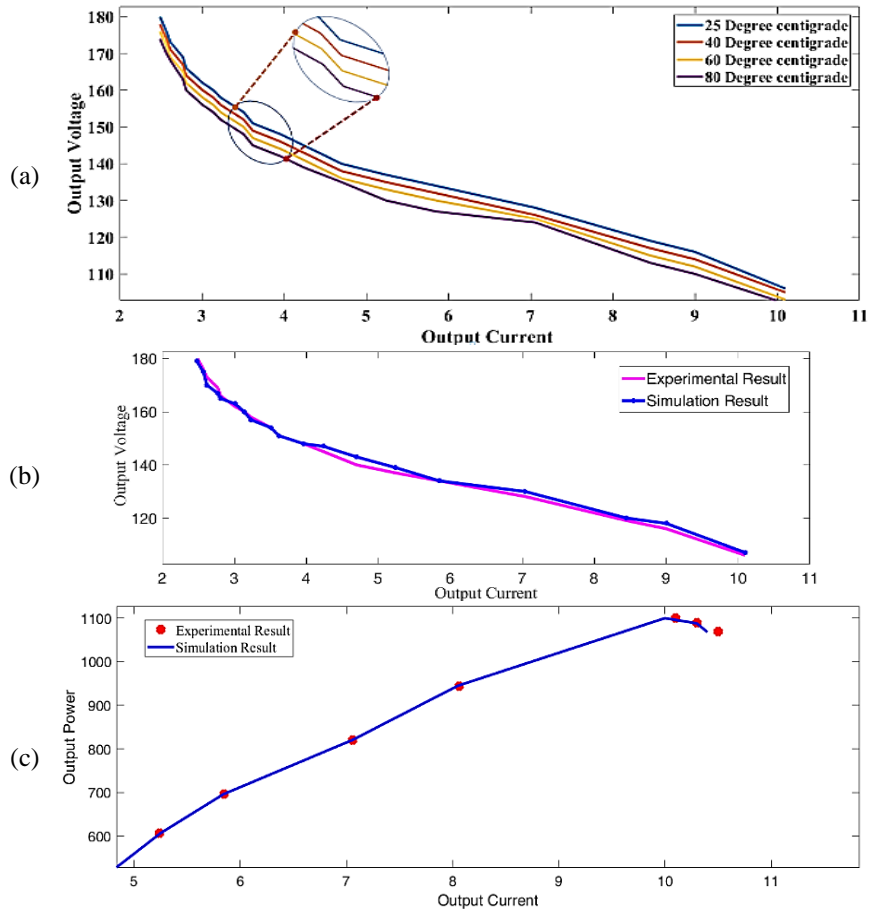


Figure 3. Validating characteristic of fuel cell: (a) variation in voltage with temperature, (b) variation of voltage with the load current, and (c) variation of power with the load current

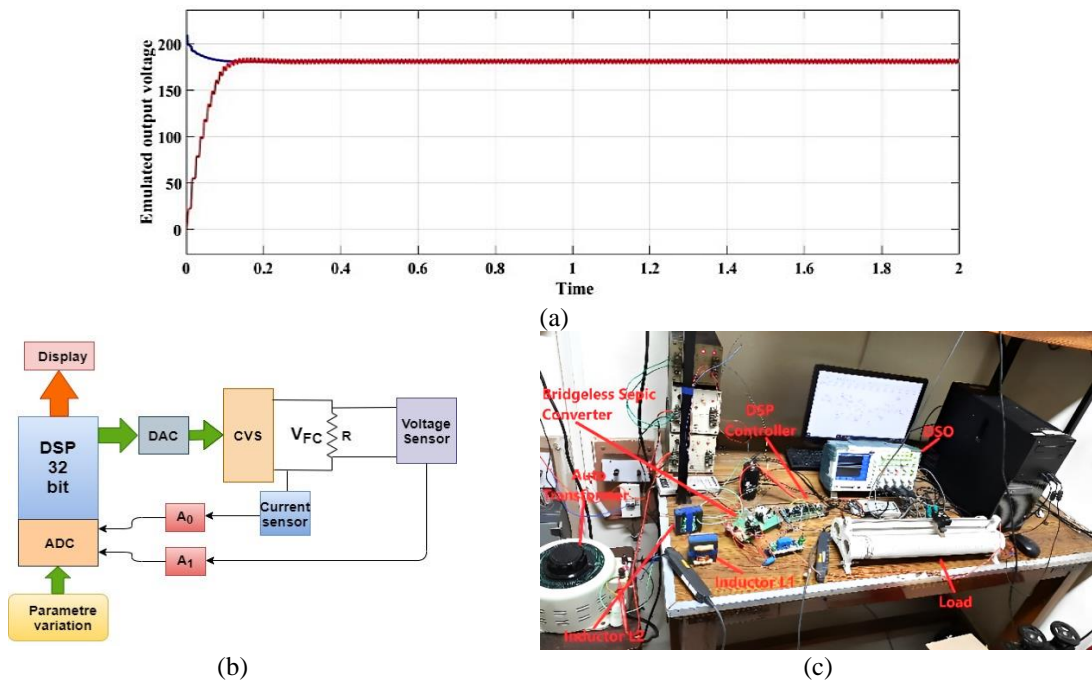


Figure 4. Fuel cell control and setup: (a) block diagram representation of interfacing software with hardware, (b) experimental setup of FC emulator, and (c) waveform of emulated output voltage

Figure 5(a), depicts the current and voltage waveforms during the operation of the power electronics converter with a 55% duty cycle. In Figure 4(b), the voltage and current of the proton exchange membrane (PEM), the output voltage of the Power Electronics Controller (PEC), and the control signal applied to the BSC sepic converter regulation are presented. The input current of the converter, denoted as I_{in} , exhibits a sinusoidal waveform current draw from (AC) source. This current waveform is in phase with input voltage V_{in} . Deviations from the optimal duty cycle (D) will position the operating point at lower power levels. In such instances, an algorithm capable of dynamically tracking the maximum output power 950 W.

Prototype emulator hardware result and simulation result both are comparable and replicate the dynamic performance of the PEMFC system. For efficient working of prototype emulator inductor L_1 and L_2 of BSC inductor L_1 working as continuous conduction mode (CCM) and inductor L_2 working in discontinuous mode (DCM). The proper design of the converter reduces ripple at the output side of the emulated voltage presented in Figure 4(a). At 25 °C temperature, 0.5 atm pressure of H_2 and 0.2 atm pressure of O_2 at a particular number of stacks generate 179 V. The result was obtained by varying the load between 10 to 95 ohm and the corresponding variation of the duty cycle varied between 0.2 to 0.6. Figure 5(b) shows the input voltage and current waveform which is in phase. The laboratory setup for testing is shown in Figure 4(c). The system's dynamic performance was evaluated, and the results are presented in Figures 5(c) and 5(d). In Figure 5(c), a decrease in current is observed with a change in load, while the voltage shows a rising when fall in current. Similarly, Figure 5(d) illustrates an increase in current alongside a decrease in the output voltage of the emulated fuel cell. These results validate the behavior of the fuel cell model. The obtained results distinctly demonstrate the emulation of fuel cell behavior, closely resembling that of a real fuel cell model.

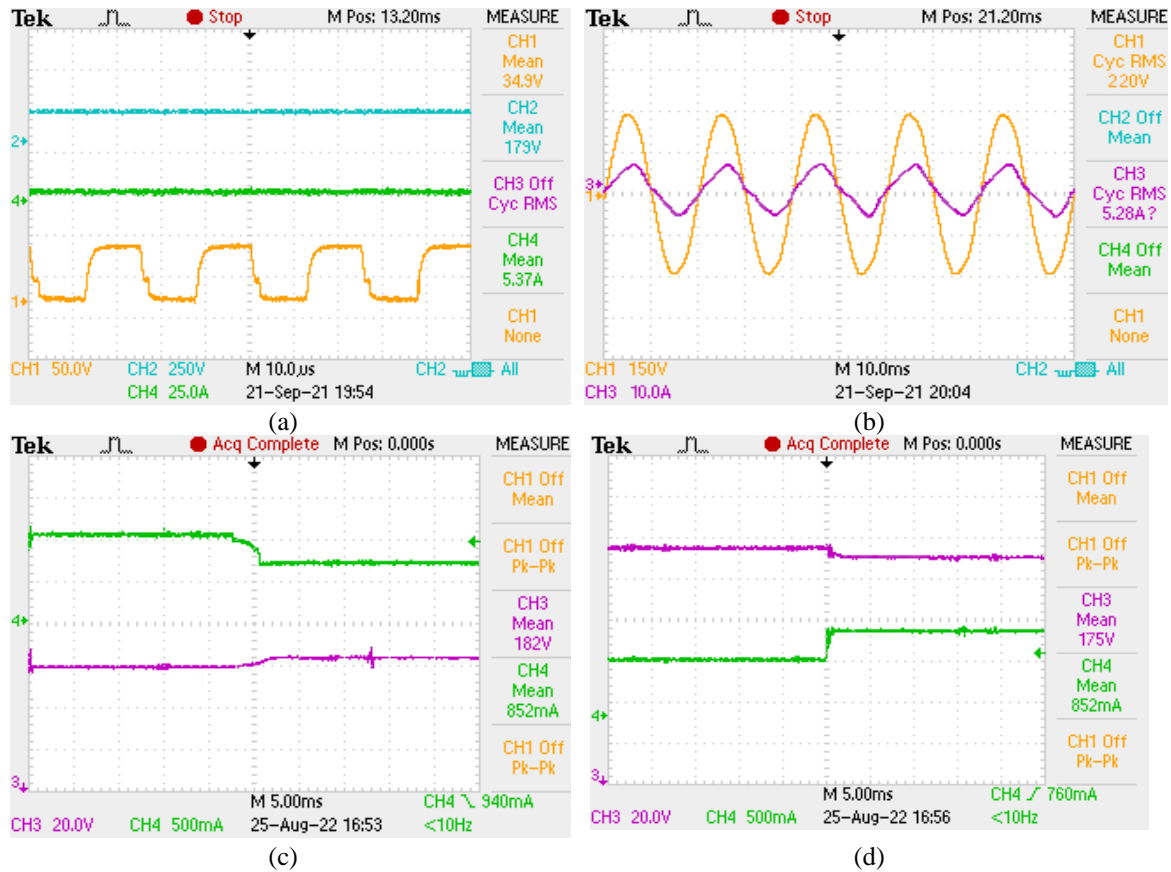


Figure 5. Hardware results: (a) waveform of input voltage and input current, (b) waveform of output voltage-output current, (c) output voltage increase and current decrease, and (d) output voltage decrease and current increase

5. CONCLUSION

This paper focuses on emulating the characteristics of a proton exchange membrane fuel cell (PEMFC) through the implementation of a coded model of (PEMFC). The analysis, modeling, and

development of a PEMFC emulator with adjustable stacks and parameters have been conducted. The resulting emulator effectively replicates the curve characteristics and operating points of a PEMFC. Furthermore, the desired power factor correction at the input side of the BSC and a ripple-free output voltage are achieved. The developed prototype, operating at 950 W, attains a power factor of 0.994. The developed setup takes less space and is low in weight, that is why it is easily portable. The advantage of this emulator is that the output voltage is easily adjustable, controllable, and scalable.

ACKNOWLEDGMENT

The authors would like to express their heartfelt gratitude to the Science and Engineering Research Board, India for their financial support under SERB POWER FELLOWSHIP Grant no. SPF/2021/000071 and SERB Project Grant no. EEQ/2021/000057.




REFERENCES

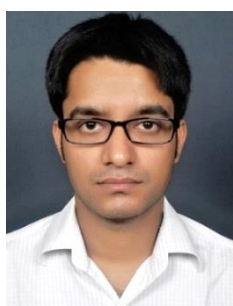
- [1] K. Chaudhary, K. Bhardvaj, and A. Chaudhary, "A qualitative assessment of hydrogen generation techniques for fuel cell applications," *Fuel*, vol. 358, no. PA, p. 130090, 2024, doi: 10.1016/j.fuel.2023.130090.
- [2] K. A. Singh, A. Prajapati, and K. Chaudhary, "High-Gain Compact Interleaved Boost Converter With Reduced Voltage Stress for PV Application," *IEEE Journal of Emerging and Selected Topics in Power Electronics*, vol. 10, no. 4, pp. 4763–4770, Aug. 2022, doi: 10.1109/JESTPE.2021.3120802.
- [3] A. Prajapati, V. Bharadwaj, and K. Chaudhary, "Isolated DC Microgrid Operation with Hybridization of PV, FC, and Battery," in *ITEC-India 2023 - 5th International Transportation Electrification Conference: eAMRIT - Accelerating e-Mobility Revolution for India's Transportation*, 2023, pp. 1–6. doi: 10.1109/ITEC-India59098.2023.10471446.
- [4] A. Prajapati and K. Chaudhary, "Analysis and Design of Integrated Boost-Luo Converter with Reduced Voltage Stress for Renewable Application," *IEEE Journal of Emerging and Selected Topics in Industrial Electronics*, vol. PP, pp. 1–12, 2024, doi: 10.1109/jestie.2024.3365388.
- [5] A. Prajapati, P. Singh, and K. Chaudhary, "Non-Isolated High Gain Bipolar Converter For Renewable Application," in *2023 IEEE International Conference on Power Electronics, Smart Grid, and Renewable Energy: Power Electronics, Smart Grid, and Renewable Energy for Sustainable Development, PESGRE 2023*, 2023, pp. 1–6. doi: 10.1109/PESGRE58662.2023.10404372.
- [6] R. M. Elavarasan *et al.*, "A Comprehensive Review on Renewable Energy Development, Challenges, and Policies of Leading Indian States with an International Perspective," *IEEE Access*, vol. 8, pp. 74432–74457, 2020, doi: 10.1109/ACCESS.2020.2988011.
- [7] M. K. Singla, P. Nijhawan, and A. S. Oberoi, "Hydrogen fuel and fuel cell technology for cleaner future: a review," *Environmental Science and Pollution Research*, vol. 28, no. 13, pp. 15607–15626, 2021, doi: 10.1007/s11356-020-12231-8.
- [8] J. K. Kuo and C. F. Wang, "An integrated simulation model for PEM fuel cell power systems with a buck DC-DC converter," *International Journal of Hydrogen Energy*, vol. 36, no. 18, pp. 11846–11855, 2011, doi: 10.1016/j.ijhydene.2011.05.107.
- [9] G. Marsala, M. Pucci, G. Vitale, M. Cirrincione, and A. Miraoui, "A prototype of a fuel cell PEM emulator based on a buck converter," *Applied Energy*, vol. 86, no. 10, pp. 2192–2203, 2009, doi: 10.1016/j.apenergy.2008.12.028.
- [10] M. Azri, N. H. A. Khanipah, Z. Ibrahim, and N. A. Rahim, "Fuel cell emulator with MPPT technique and boost converter," *International Journal of Power Electronics and Drive Systems*, vol. 8, no. 4, pp. 1852–1862, 2017, doi: 10.11591/ijpeds.v8i4.pp1852-1862.
- [11] V. Sanchez, F. Chan, J. M. Ramirez, and J. C. Rosas-Caro, "Fuel cell emulator based on interleaved synchronous buck converter," in *2012 IEEE Energy Conversion Congress and Exposition, ECCE 2012*, 2012, pp. 4464–4470. doi: 10.1109/ECCE.2012.6342214.
- [12] P. M. García-Vite, B. L. Reyes-García, C. L. Valdez-Hernández, and A. L. Martínez-Salazar, "Microcontroller-based emulation of a PEM fuel cell," *International Journal of Hydrogen Energy*, vol. 45, no. 26, pp. 13767–13776, 2020, doi: 10.1016/j.ijhydene.2019.10.034.
- [13] C. De Beer, P. Barendse, and A. Khan, "Development of an HT PEM fuel cell emulator using a multiphase interleaved DC-DC converter topology," *IEEE Transactions on Power Electronics*, vol. 28, no. 3, pp. 1120–1131, 2013, doi: 10.1109/TPEL.2012.2208481.
- [14] F. M. Guangel and G. T. Chala, "A comparative study between the seven types of fuel cells," *Applied Science and Engineering Progress*, vol. 13, no. 3, pp. 185–194, 2020, doi: 10.14416/J.ASEP.2020.04.007.
- [15] A. Mohammadi, G. Cirrincione, A. Djerdir, and D. Khaburi, "A novel approach for modeling the internal behavior of a PEMFC by using electrical circuits," *International Journal of Hydrogen Energy*, vol. 43, no. 25, pp. 11539–11549, Jun. 2018, doi: 10.1016/j.ijhydene.2017.08.151.
- [16] A. Saadi, M. Becherif, D. Hissel, and H. S. Ramadan, "Dynamic modeling and experimental analysis of PEMFCs: A comparative study," *International Journal of Hydrogen Energy*, vol. 42, no. 2, pp. 1544–1557, Jan. 2017, doi: 10.1016/j.ijhydene.2016.07.180.
- [17] A. A. Fardoun, H. A. N. Hejase, A. Al-Marzouqi, and M. Nabag, "Electric circuit modeling of fuel cell system including compressor effect and current ripples," *International Journal of Hydrogen Energy*, vol. 42, no. 2, pp. 1558–1564, 2017, doi: 10.1016/j.ijhydene.2016.07.093.
- [18] S. L. Chavan and D. B. Talange, "Modeling and performance evaluation of PEM fuel cell by controlling its input parameters," *Energy*, vol. 138, pp. 437–445, 2017, doi: 10.1016/j.energy.2017.07.070.
- [19] Z. Abdin, C. J. Webb, and E. M. A. Gray, "PEM fuel cell model and simulation in Matlab–Simulink based on physical parameters," *Energy*, vol. 116, pp. 1131–1144, 2016, doi: 10.1016/j.energy.2016.10.033.
- [20] A. Omran *et al.*, "Mathematical model of a proton-exchange membrane (PEM) fuel cell," *International Journal of Thermofluids*, vol. 11, 2021, doi: 10.1016/j.ijft.2021.100110.
- [21] J. M. Corrêa, F. A. Farret, V. A. Popov, and M. G. Simões, "Sensitivity analysis of the modeling parameters used in simulation of proton exchange membrane fuel cells," *IEEE Transactions on Energy Conversion*, vol. 20, no. 1, pp. 211–218, 2005, doi: 10.1109/TEC.2004.842382.
- [22] P. T. Moseley, "Fuel Cell Systems Explained," *Journal of Power Sources*, vol. 93, no. 1–2, p. 285, 2001, doi: 10.1016/s0378-7753(00)00571-1.




- [23] B. Singh and V. Bist, "Improved power quality bridgeless Cuk converter fed brushless DC motor drive for air conditioning system," *IET Power Electronics*, vol. 6, no. 5, pp. 902–913, 2013, doi: 10.1049/iet-pe.2013.0050.
- [24] K. A. Singh and K. Chaudhary, "Design and development of a new three-phase AC-DC single-stage wind energy conversion system," *IET Power Electronics*, vol. 14, no. 2, pp. 302–312, Feb. 2021, doi: 10.1049/pe.2021.12034.
- [25] Y. Liu, Y. Sun, and M. Su, "A Control Method for Bridgeless Cuk/SePIC PFC Rectifier to Achieve Power Decoupling," *IEEE Transactions on Industrial Electronics*, vol. 64, no. 9, pp. 7272–7276, 2017, doi: 10.1109/TIE.2017.2688979.

BIOGRAPHIES OF AUTHORS






Ashish Prajapati    received the B.E. degree in electrical engineering from the Rajkiya Engineering college, Banda, India, in 2016, and the M.Tech. degree in electrical drives, in 2019, from the Maulana Azad National Institute of Technology Bhopal, Madhya Pradesh, India. Currently, he is working toward a Ph.D. degree in electrical engineering from the Indian Institute of Technology (Banaras Hindu University), Varanasi, Uttar Pradesh, India. His research interests are high gain DC/DC converters, renewable energy integration in DC microgrids, solar and fuel cell hybrid energy systems, and multiport converters. He can be contacted at email: ashishprajapati.rs.eee19@itbhu.ac.in.



Tripurari Das Gupta    is currently an Assistant Professor in the Department of Electrical and Electronics Engineering, Nalanda College of Engineering, Nalanda, India. He completed his Ph.D. degree from the Department of Electrical Engineering, Indian Institute of Technology (BHU) Varanasi, India in 2021. His current research interests include design and analysis of switched reluctance machines and the analysis of fuel cell systems. He can be contacted at email: tripu008@gmail.com.



Kalpana Chaudhary    received the Ph.D. degree in electrical engineering from the Indian Institute of Technology (Banaras Hindu University), Varanasi, Uttar Pradesh, India, in 2009. She is currently an Associate Professor with the Department of Electrical Engineering, Indian Institute of Technology (Banaras Hindu University). She has more than twenty years of teaching and research experience. She has supervised four Ph.D. thesis and 52 M.Tech. dissertations. She is the Principal Investigator of two research projects sponsored by the Government of India. She has authored or co-authored more than 40 scientific articles, book chapters, and research papers in indexed international journals and prestigious conference proceedings, a book as a sole author, and three book chapters. She can be contacted at email: kchaudhary.eee@itbhu.ac.in.